Measurement of high-dynamic temperature field using high-speed quadriwave lateral shearing interferometer*

CUI Bo-chuan (崔博川)[1,2], **WANG Jian-li** (王建立)[1]**, **YAO Kai-nan** (姚凯男)[1], **and CHEN Tao** (陈涛)[1]

1. Changchun Institute of Optics, Fine Mechanics and Physics, Chinese Academy of Sciences, Changchun 130033, China

2. University of Chinese Academy of Sciences, Beijing 100049, China

(Received 26 September 2017)

An approach to measure a high-dynamic two-dimensional (2D) temperature field using a high-speed quadriwave lateral shearing interferometer (QWLSI) is proposed. The detailed theoretical derivation to express the wavefront reconstruct principle of the proposed method is presented. The comparison experiment with thermocouples shows that the temperature field measurement using QWLSI has a precision of ±0.5 °C. An experiment for measuring the high-dynamic temperature field generated by an electrical heater is carried out. A 200 frame rate temperature field video with 512 × 512 resolution is obtained finally. Experimental results show that the temperature field measurement system using a QWLSI has the advantage of high sensitivity and high resolution.

Document code: A **Article ID:** 1673-1905(2018)02-0124-5

DOI https://doi.org/10.1007/s11801-018-7218-7

Temperature measurement is one of the most concerned issues in the measurement of flame parameters. The temperature not only includes the chemical reaction process, but also suggests the influence of the flow field on the flame. Flame is something complex in the fluid field, involving fluid dynamics, chemical reaction dynamics and so on[1]. The measurement of flame temperature is difficult. Thermocouple, hot wire anemometer and other contact measurement methods were first used in the measurement of flame temperature. But the method of contact measurement would disturb the flow field, so it is not an ideal way for measuring flow field, especially in the laboratory, where the geometry of measured flame is small.

With the development of science and technology, many non-contact flow field measurement methods are found. In 1970s, laser speckle density photography were applied to the measurement of flame parameters. At the beginning of the twenty-first century, Richard and Meier[2] reported background-oriented schlieren (BOS) technique based on the visualization of traditional schlieren images. In recent years, some composite approaches were proposed for obtaining reliable measurements of complex temperature fields. In 2015, a long period grating concatenated with multimode fiber which was used for simultaneous measurement of temperature was introduced[3]. In 2016, a combination of the visible image processing technique and the spectroscopic line-ratio method at two specified wavelengths was proposed to measure the two-dimensional (2D) temperature filed of thermal plasmas[4]. In 2017, a background-oriented schlieren tomography for the temperature field reconstruction in a non-isothermal swirling jet undergoing vortex breakdown was proposed[5]. At the same year, the shock oscillations of transonic flying objects was tracked using background-oriented schlieren technique[6].

However, traditional non-contact flow field measurement method depends on the digital image process technology[7]. It is difficult to measure the temperature with a high precision. It is also prone to generate error in the measurement of temperature boundary layer. So a high-precise and compact non-contact method to measure the temperature field is needed.

The concept of the quadriwave lateral shearing interferometer (QWLSI) was proposed in 2000 and is based on the interference of four tilted replicas of the wavefront to be analyzed[8-11]. The QWLSI offers the crucial advantage that it yields an analyzed wavefront without the use of a reference arm and consequent time consuming alignment. It combines fundamental properties, such as the achromaticity, the high resolution, the adjustable sensitivity and dynamic, to a great versatility. Due to these qualities, the QWLSI is an excellent candidate to perform high quality wavefront measurements in hard context.

In this paper, we introduce QWLSI into the temperature field measurement. A high-speed QWLSI is used to measure high-dynamic temperature field. Good results of temperature field are measured with 200 frame

* This work has been supported by the National Natural Science Foundation of China (No.11603024).

** E-mail: icysmart@mail.ustc.edu.cn

rate and ±0.5 °C error. This approach extends the method of temperature field measurement, which is of great significance to the study of aerodynamics and kinetics of flame and so on.

Lateral shearing interferometry is a well-known technique to measure the phase gradients in one direction. The incident wavefront is replicated into two identical but tilted wavefronts. After propagation, their mutual interference pattern is recorded by a CCD camera. The phase gradients are recovered from the fringe deformation, by means of a Fourier deconvolution around the interferogram fringe frequency. However, at this point, it lacks some gradient information to recover a full 2D phase field. Multiwave interferometry[12,13] extends this principle to more than one gradient direction. In the case of QWLSI, as shown in Fig.1, four replicas are created by a specific 2D diffraction grating. In this case, two gradients along two perpendicular directions are measured and then integrated to determine the field intensity and phase[9].

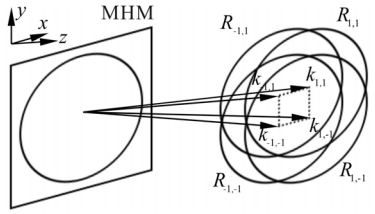

$\boldsymbol{k}_{i,j}$: the wave vector; $R_{i,j}$: the corresponding intensity pattern

Fig.1 Principle of the quadriwave lateral shearing interference

Fig.2 shows the computational process of temperature field measurement using QWLSI. First of all, demodulate the interferogram to calculate the optical path difference (*OPD*). According to the refraction law, the relationship between *OPD* and refractive index *n* is

$$nL=OPD, \tag{1}$$

where *L* is the propagation length.

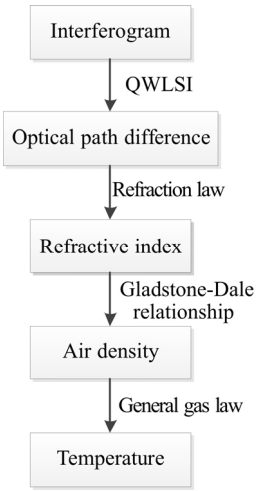

Fig.2 Flow chart of temperature field measurement

Then we use Gladstone-Dale relationship to calculate the air density ρ:

$$n=\kappa\rho+1, \tag{2}$$

where κ is the Gladstone-Dale constant, and its value depends on the component of air and wavelength[14].

Finally, the air density and temperature can be linked through the general gas law. When the atmosphere pressure keeps unchanging, the relationship between the air density and the temperature is

$$\rho T=\rho_0 T_0, \tag{3}$$

where ρ_0 is the density of air in ambient temperature T_0.

The interferogram deformation can be interpreted using either the wave or geometrical optics. Wave optics is more rigorous and underlies the interferogram numerical processing, whereas geometrical optics is more intuitive to understand physical effects, such as the influence of spatial coherence on interferogram contrast.

A diffraction grating replicates the incident beam. In the case of our QWLSI, the so-called modified Hartmann mask (MHM) is used[15]. It is made of the superposition of a Hartmann mask (with amplitude grating period of *p*) and a p-shift checker board (with phase grating period of 2*p*) as presented in Fig.3. This is optimized to diffract more than 90% of the light energy into the 4 first orders carried by 4 wave vectors.

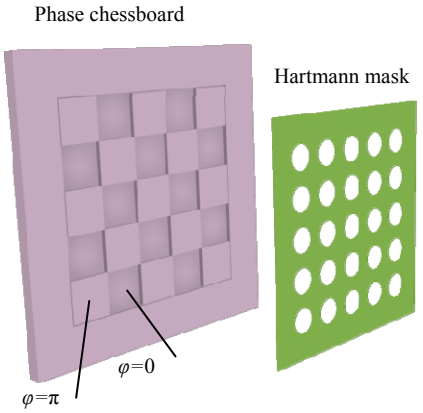

Fig.3 The construction of MHM

If only the 4 first orders are considered, the amplitude transmittance of the perfect MHM is given by

$$t(x,y)=\cos(\frac{\pi x}{p})\cdot\cos(\frac{\pi y}{p}). \tag{4}$$

After a propagation length *z* along the *z*-axis, in the scope of paraxial propagation and if we neglect free space diffraction, the electromagnetic field is the coherent addition of all the replicas, which are mutually displaced due to their deviation. The intensity is given by

$$I(r,z)=I_0\left\{1+[\cos(\frac{2\pi}{p}x+\frac{2\pi}{p}z\frac{\partial OPD}{\partial x})+\cos(\frac{2\pi}{p}y+\frac{2\pi}{p}z\frac{\partial OPD}{\partial y})\right]+\frac{1}{2}\left[\cos(\frac{2\pi}{p}(x+y)+\right.$$

$$\frac{2\pi}{p}z\frac{\partial OPD}{\partial(x+y)})+\cos\left(\frac{2\pi}{p}(x-y)+\frac{2\pi}{p}z\frac{\partial OPD}{\partial(x-y)}\right)\Bigg]\Bigg\} \quad (5)$$

After the interferogram is obtained by our CCD, the fast Fourier transform (FFT) and the differential Zernike polynomial fitting method can be employed for wavefront retrieval[16,17]. As shown in Fig.4, the interferogram is at first transformed into the Fourier spectrum by FFT. Then the +1 orders in the x and y directions are selected and transformed into the shearing wavefronts in the x and y directions by inverse fast Fourier transform (IFFT), respectively[18]. Last, the differential Zernike polynomial fitting method is employed to retrieve the actual wavefront distribution using these two orthogonal shearing wavefronts.

Supposing that the *OPD* under test is $W(x, y)$, these two shearing wavefronts obtained by Fourier spectral filtering and IFFT can be expressed as

$$\Delta W_x(x,y)=W(x-\frac{s}{2},y)-W(x+\frac{s}{2},y) \quad (6)$$

$$\Delta W_y(x,y)=W(x,y-\frac{s}{2})-W(x,y+\frac{s}{2}) . \quad (7)$$

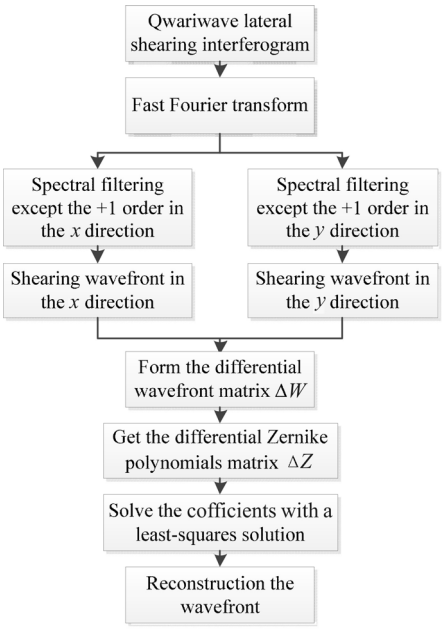

Fig.4 *OPD* retrieval method using FFT and differential Zernike polynomial fitting

In modal wavefront retrieval, the wavefront is decomposed into a set of basic functions, while Zernike polynomials are commonly used as the basic functions for this retrieval. The original wavefront $W(x, y)$ can be explained by N terms of Zernike polynomials in the following form,

$$W(x,y)=\sum_{j=1}^{N}a_jZ_j(x,y) . \quad (8)$$

Substituting Eq.(8) into Eq.(6) and (7), the shearing wavefronts expressed in the form of Zernike polynomials can be obtained as

$$\Delta W_x(x,y)=\sum\nolimits_{j=1}^{N}a_j\left[Z_j(x-\frac{s}{2},y)-Z_j(x+\frac{s}{2},y)\right] , \quad (9)$$

$$\Delta W_y(x,y)=\sum\nolimits_{j=1}^{N}a_j\left[Z_j(x,y-\frac{s}{2})-Z_j(x,y+\frac{s}{2})\right] . \quad (10)$$

If the differential Zernike polynomials are defined as

$$\Delta Z_x=Z_j(x-\frac{s}{2},y)-Z_j(x+\frac{s}{2},y) , \quad (11)$$

$$\Delta Z_y=Z_j(x,y-\frac{s}{2})-Z_j(x,y+\frac{s}{2}) , \quad (12)$$

the shearing wavefronts $W_x(x, y)$ and $W_y(x, y)$ can be expressed as

$$\begin{pmatrix}\Delta W_x\\ \Delta W_y\end{pmatrix}=\begin{pmatrix}\Delta Z_x\\ \Delta Z_y\end{pmatrix}\boldsymbol{a} . \quad (13)$$

Now the coefficients of Zernike polynomials can be obtained with the least-squares solution, that is,

$$\boldsymbol{a}=(\Delta\boldsymbol{Z}^{\mathrm{T}}\Delta\boldsymbol{Z})^{-1}\Delta\boldsymbol{Z}^{\mathrm{T}}\Delta\boldsymbol{W} , \quad (14)$$

Substituting the coefficients obtained from Eq.(14) into Eq.(8), we can finally retrieve the wavefront under test.

The QWLSI is shown as Fig.5(a). It includes an MHM and a CCD. The aperture period of Hartmann diaphragm p is 11 μm, and the CCD pixel size is 5.5 μm. The resolution of CCD is 2 048×2 048, which means the maximum resolution of phase image is 512×512. Fig.5(b) is an interferogram obtained by this shearing interferometer.

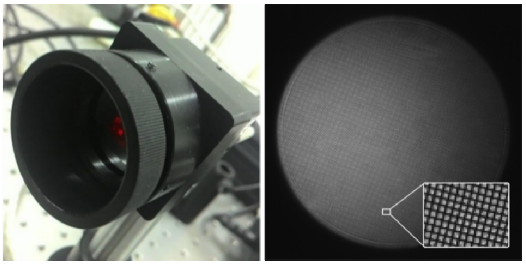

(a) (b)

Fig.5 (a) Photo of QWLSI and (b) an interferogram obtained by this QWLSI

Fig.6 shows the optical systems of the temperature field measurement. A He-Ne laser is used to produce spatial coherence source of light. An aplanatic lens L_1 collimates the incident beam into plane wavefronts. F_1 is the temperature field under test. The air density can be mutative due to the uneven temperature distribution. L_2 and L_3 are a beam contracting system so that the interferometer can obtain the interferogram of the whole temperature field under test.

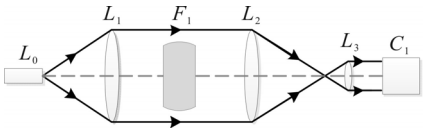

L_0: He-Ne laser with λ=450 nm; L_1 and L_2: aplanatic lens with f=50 mm; F_1: Temperature field under test; L_3: aplanatic lens f=20 mm; C_1: QWLSI

Fig.6 Schematic diagram of optical systems

The MHM can also be considered as a grid of holes, and the classical interpretation of Hartmann and Shack-Hartmann wavefront sensors can be used. The incident wavefront is sampled by the Hartmann holes. We record the projection of the holes in the CCD plane. Fig.7(a) shows an interferogram formed by a plane wave, and Fig.7(b) is a disturbed one.

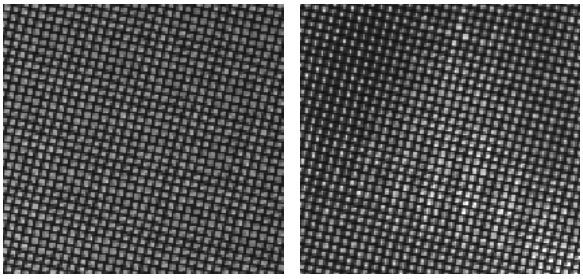

Fig.7 Interferograms obtained by the QWLSI formed by (a) plane wave and (b) disturbed wave due to the air with uneven density

In order to get the accuracy of the temperature field measurement using QWLSI. A set of control experiments was designed. As shown in Fig.8, the liquid in a square vessel heated by a heater was used to maintain a static temperature field. Then an Omega RHXL3SD thermocouple was used to compare the experimental results. Fig.9 shows the temperature section distribution and the comparison results thermocouple and QWLSI. The precision of the thermocouple for measuring the temperature is ±0.5 °C. Therefore, the error of temperature field measurement results using QWLSI in no more than 0.5 °C.

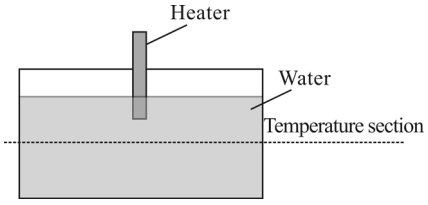

Fig.8 Schematic diagram of the temperature contrast experimental setup

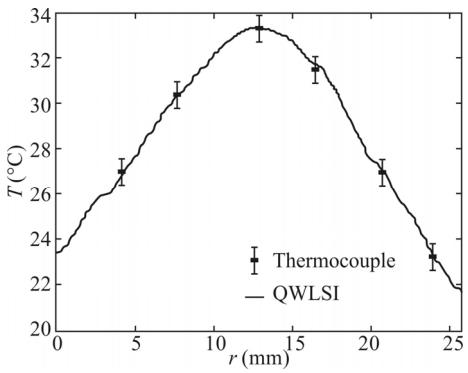

Fig.9 Comparison results of temperature field obtained by the thermocouple and the QWLSI

An electrical heater was used to change the temperature field. And a QWLSI was used to detect the *OPD*. Then the distribution of temperature field can be calculated by the process shown in Fig.2. The shape of the electrical heater is shown in Fig.10(a), and the temperature field is shown in Fig.10(b). The image size of the temperature field is 512 pixel×512 pixel, where each pixel has a side length of 0.15 mm. The sensitivity of temperature is 0.1 °C. This experiment shows that our temperature field measurement system using a QWLSI has high sensitivity and high resolution.

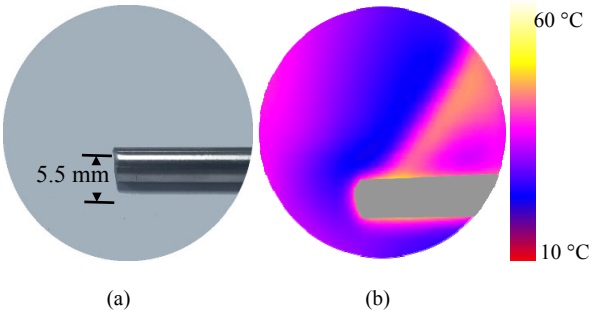

Fig.10 (a) Electrical heater and (b) the temperature field generated by the electrical heater

In conclusion, an approach to measure the varying temperature field using a QWLSI is proposed in this paper. Specific procedures for temperature field measurements using QWLSI are presented. Zernike polynomial fitting method is employed to retrieve the *OPD* from the interferogram. Gladstone-Dale relationship and general gas law are used to calculate the distribution of the temperature field. An experiment for measuring the certain temperature field produced by an electrical heater is carried out. Experimental results show that using a QWLSI to measure the temperature field has the advantage of high sensitivity and high resolution.

In the next step, we will use a Bunsen burner with a mixture of combustible gases as a source for temperature field measurements. Thermocouples will also be used for verification. Then, we will reconstruct the 3D temperature field using QWLSI.

References

[1] A. Yule, N. Chigier, S. Ralph, R. Boulderstone and J. Venturag, AIAA Journal **19**, 752 (2015).

[2] H. Richard and M. Raffel, Measurement Science and Technology **12**, 1576 (2001).

[3] Y. Miao, H. Zhang, J. lin, B. Song, K. Zhang, W. Lin, B. Liu and J Yao, Applied Physics Letters **106**, 132410 (2015).

[4] H. Guo, P. Li, H. Li, N. Ge and C. Bao, Review of Scientific Instruments **87**, 033502 (2016).

[5] H. Lang, K. Oberleithner, C. Paschereit and M. Sieber, Experiments in Fluids **58**, 88 (2017).

[6] T. Sueishi, M. Ishii and M. Ishikawa, Applied Optics **56**, 3789 (2017).

[7] F. Nicolas, V. Todoroff, A. Plyer, G. Besnerais, D. Donjat, F. Micheli, F. Champagnat, P. Cornic and Y. Le Sant, Experiments in Fluids **57**, 13 (2016).

[8] J. Ren, X. Luo, A. Xia and Y. Zhang, Applied Mechanics & Materials **568-570**, 50 (2014).

[9] Yue Xiumei, Yang Yonging, Ling Tong, Liu Dong, Luo Yandong, Bai Jian and Shen Yibing, Chinese Journal of Lasers **42**, 1008006 (2015).

[10] S. Aknoun, P. Bon, J. Savatier, B. Wattellier and S. Monneret, Optics Express **23**, 16383 (2015).

[11] S. Aknoun, J. Savatier, P. Bon, F. Galland, L. Abdeladim, B. Wattellier and S. Monneret, Journal of Biomedical Optics **20**, 126009 (2015).

[12] X. Chen, L. Dong, S. Wang, P. Yang and B. Xu, Optics Communications **402**, 276 (2017).

[13] W. Zhu, J. Li, L. Chen, D. Zheng, Y. Yang and Z. Han, Optics Communications **380**, 214 (2016).

[14] S. Monneret, P. Bon, G. Baffou, P. Berto, J. Savatier, S. Aknoun and H. Rigneault, Proceedings of the SPIE **8792**, 879209 (2013).

[15] J. Primot and N. Guerineau, Applied Optics **39**, 5715 (2000).

[16] F. Dai, F. Tang, X. Wang, O. Sasaki and P. Feng, Applied Optics **51**, 5028 (2012).

[17] T. Ling, D. Liu, L. Sun, Y. Yang and Z. Cheng, Proceedings of the SPIE **8838**, 88380J (2013).

[18] H. Ina, M. Takeda and S. Kobayashi, Journal of the Optical Society of America **72**, 156 (1982).